High-Field Saturation Properties of the Ion Atmosphere Polarization Surrounding a Rigid, Immobile Rod

Donald C. Rau* and Elliot Charney

Laboratory of Chemical Physics, National Institute of Arthritis, Diabetes, and Digestive and Kidney Diseases, National Institutes of Health, Bethesda, Maryland 20205.
Received November 19, 1982

ABSTRACT: We have extended our treatment of the electric polarization of a Debye–Hückel ion atmosphere surrounding a fixed, charged rod to high applied fields as a first-order model for the dipole saturation properties of rigid polyelectrolytes, particularly DNA. In contrast to the commonly assumed saturating induced dipole model, in which dipole moments are linearly proportional to the field strength, E, at low fields and saturate to a constant value at sufficiently large field strengths, the theory developed here indicates that the dipole moment will attain a maximal value and then decrease as the applied field strength is increased further. This unusual behavior is related to the Wien effect in electrophoresis and is due to the progressive stripping of the ion atmosphere away from the electrostatic influence of the central rod. Several features of the high-field orientation behavior of DNA can be qualitatively reproduced by the theory. Most importantly, the theory can give an unusually long, high-field region of approximately linear dependence of the orientation on $1/E$ and infinite field extrapolations of the orientation (or apparent optical parameter) that are dependent on DNA length.

Introduction

Electric dichroism is becoming an increasingly important tool for investigating the structure of biologically important macromolecules (e.g., ref 1 and 2). One capability of the technique is the determination of the orientation of the optical axis with respect to the electrical axis by extrapolating the observed dichroism to infinite field strength. Only for classical permanent and induced dipole moments, however, has the form of the extrapolation function been theoretically determined.[3,4] A number of polyelectrolytes, however, have dipole properties that do not conveniently fall into either category. Most commonly, at low applied field strengths, the dipole appears to be purely induced, with moments that are linearly proportional to E; i.e., the electric polarizability is constant. At higher fields, however, the polarizability apparently decreases, leading to dipole moments that are increasing at a rate slower than linear with E. This effect is generally termed dipole saturation. Since the high-field behavior of the dichroism or birefringence of the biological polyelectrolyte DNA has been extensively studied, we restrict out comparison of theory and experiment to DNA. Empirically, for short rodlike fragments of DNA, at high field strengths, the observed dichroism varies linearly with $1/E$ once the dichroism reaches about 50% of the extrapolated value.[1,5,6] Since the dipole moment of DNA is known to be induced, it is generally accepted that this linear $1/E$ dependence at high fields reflects a substantial saturation of the induced dipole moment. Current attempts to fit the orientation function[7-10] have assumed that the induced dipole moment saturates at high field strengths to a value that is independent of E, i.e., to a permanent-like dipole moment. Applying this approach to DNA has resulted in several problems. It is difficult to theoretically mimic the experimentally observed extensive region of linear $1/E$ dependence. Secondly, the extrapolated, infinite-field dichroism is significantly smaller than would be predicted on the basis of the "classical" B-form structure.[1,11,12] It furthermore appears that the limiting dichroism is dependent on the molecular weight of the DNA.[11,12] Lastly, in contrast to Kerr region field strengths, for which the induced dipole moment apparently varies with L^2, where L is the DNA length,[1,6,12,13] the high-field limiting dipole moment is substantially independent of the size of the DNA, a feature of the extrapolation that has not been predicted by theory.[6,12]

Given the inverse dependence of the dipole moment of DNA on the ionic strength of the solution, it is generally accepted now that the orientation is due to the polarization of the surrounding small ions relative to the long axis of the DNA helix. Although somewhat artificial, the polarization can be broken down into two components, the induced dipole moment due to the condensed counterion layer and that due to the polarization of the surrounding diffuse atmosphere. Most treatments for the saturation of the condensed counterion dipole implicitly assume that the number of counterions on the DNA interacting with the field remains constant, resulting in high-field limiting dipole moments that are independent of the field strength E, i.e., a permanent-like dipole, but then predict that this limiting dipole will depend on the length of DNA.[7-10] We have recently calculated the dipole moment due to the polarization of a Debye–Hückel ion atmosphere surrounding a charged rod in the low-field limit, i.e., for induced dipole energies that are proportional to E^2.[14] In an attempt to gain at least some qualitative insights into the saturation properties of an induced dipole moment that is due to the polarization of the surrounding ion atmosphere, we extend these calculations in this paper to arbitrarily high field strengths. We still treat the ion atmosphere in the Debye–Hückel limit, neglect the effect of condensed counterion polarization, and make the simplifying but incorrect assumption that the electrophoretic velocity of DNA is negligible in comparison with small ions. Although a complete description of the polarization of the small ions surrounding DNA is far more complicated than the treatment given here due to the inadequacies of the Debye–Hückel limit in describing the true ion atmosphere distribution function for a macroion as highly charged as DNA and also due to the complicated hydrodynamic interactions between moving salt ions and an electrophoresing DNA rod, we feel that a description of the dipole saturation properties for an isolated Debye–Hückel ion atmosphere will lead to a qualitatively correct picture. The most important difference between the more realistic steady-state flow model considered here and the constant counterion number, equilibrium calculations of the others[7-10] is that our results indicate that the dipole moment will not just reach a value that is independent of E, i.e.,

a permanent-like dipole moment, but rather the moment will increase with E to a *maximum* value, after which increasing E actually results in decreasing dipole moments. This unusual high-field behavior is related to the Wien effect in electrophoretic theory and experiment (e.g., ref 15). At high field strengths, the ion atmosphere is being stripped away from the central charged rod, leaving, in essence, fewer charges left to polarize in the field. This effect can result in extrapolating apparent optical parameters that do not reflect the structure of DNA.

Theory

Since the model we consider in the high-field case is identical with our previous low-field work,[14] we shall only basically outline the formalism in reaching eq 9–13. It is then at this point that the treatment diverges from the low-field work. The model we consider is that of a thin rod of radius a' and length $2L'$, uniformly charged over its surface to an effective linear charge density Qe, where Q is the linear number density of surface charges. The rod is immersed in a medium of dielectric constant ϵ, containing a simple 1–1 electrolyte with a number concentration of cations or anions n_0. Relative to the central rod and in cylindrical coordinates, the concentration distribution functions for +1 and −1 ions, $n_+(x,r)$ and $n_-(x,r)$, respectively, can be expressed in terms of the dimensionless functions $\nu_+(x,r)$ and $\nu_-(x,r)$ by

$$n_+(x,r) = n_0(1 + \nu_+(x,r))$$
$$n_-(x,r) = n_0(1 + \nu_-(x,r)) \quad (1)$$

We can further define the functions $g(x,r)$ and $f(x,r)$ as linear combinations of ν_+ and ν_-

$$g(x,r) = \nu_+(x,r) + \nu_-(x,r)$$
$$f(x,r) = \nu_+(x,r) - \nu_-(x,r) \quad (2)$$

In this form, $g(x,r)$ represents a total ion number probability distribution, while $f(x,r)$ gives a net ion charge probability function.

There are two electrostatic potentials acting on small ions in solution. One is due to the externally applied field of magnitude E'. Since it can be shown for rods sufficiently long in comparison with the Debye shielding length $1/\kappa$ that the perpendicular component of the ion atmosphere polarization is negligible with respect to the parallel component, we assume that the applied potential is then just $-E'x$. The potential ψ' is due to the distribution of charges in solution. The standard Poisson equation and boundary conditions for this internal field are

$$\nabla^2\psi'(r,x) = -4\pi e n_0 f(r,x)/\epsilon \quad (3)$$
$$\lim_{r\to\infty} \psi'(r,x) = 0 \quad (3')$$
$$\frac{\partial\psi'(a',x)}{\partial r} = 0; \quad |x| > L'$$
$$= -2Qe/\epsilon a'; \quad |x| \le L' \quad (3'')$$

In terms of these potentials and the functions $f(x,r)$ and $g(x,r)$, the steady-state flow equations and associated boundary conditions for +1 and −1 ions in solution are

$$\nabla^2 f - f = (1/2)gf - (e/kT)\nabla g\cdot\nabla\psi' + (e/kT)E'\partial g/\partial x \quad (4)$$
$$\lim_{r\to\infty} f(r,x) = 0 \quad (4')$$
$$\frac{\partial f(a',x)}{\partial r} = -(e/kT)(2 - g(a',x))\frac{\partial\psi'(a,x)}{\partial r} \quad (4'')$$

$$\nabla^2 g = (1/2)f - (e/kT)\nabla f\cdot\nabla g + (e/kT)E'\partial f/\partial x \quad (5)$$
$$\lim_{r\to\infty} g(r,x) = 0 \quad (5')$$
$$\frac{\partial g(a',x)}{\partial r} = -(e/kT)f(a',x)\frac{\partial\psi'(a',x)}{\partial r} \quad (5'')$$

At this point it is convenient to subdivide the ψ', f, and g functions into two components each. There is a component for each function that is symmetric about the x axis and can expanded in a cosine Fourier series, ψ'_+, f_+, and g_+. The functions ψ'_-, f_-, and g_- represent those components that are odd functions of the variable x and can be expanded in a sine Fourier series. As with the low-field calculations, we apply the Debye–Hückel approximation and retain only those terms in the differential equations of the lowest order of magnitude in e^2Q/kT. For the above functions, ψ'_+, f_+, and g_- all have leading linear terms (in a series expansion) in e^2Q/kT, while the lowest order for ψ'_-, f_-, and g_+ is $(e^2Q/kT)^2$. In contrast to our previous work, however, we do not restrict the equations to the lowest order of magnitude terms in $eE'\kappa/kT$. As before, we also transform to the dimensionless variables y and ρ by

$$\rho = \kappa r; \qquad y = \kappa x \quad (6)$$

where κ is the Debye shielding parameter defined by

$$\kappa^2 = 8\pi e^2 n_0/\epsilon kT \quad (7)$$

We further transform to the dimensionless potential ψ and field E by

$$\psi = e\psi'/kT; \qquad E = eE'/(\kappa kT) \quad (8)$$

Incorporating the above transformations and simplifications, we write the steady-state flow equations and boundary conditions as

$$\nabla^2 f_+ - f_+ = E\partial g_-/\partial y \quad (9)$$
$$\lim_{\rho\to\infty} f_+(\rho,y) = 0 \quad (9')$$
$$\partial f_+(a,y)/\partial\rho = -2\partial\psi_+(a,y)/\partial\rho \quad (9'')$$
$$\nabla^2 g_- = E\partial f_+/\partial y \quad (10)$$
$$\lim_{\rho\to\infty} g_-(\rho,y) = 0 \quad (10')$$
$$\partial g_-(a,y)/\partial\rho = 0 \quad (10'')$$
$$\nabla^2 g_+ = \tfrac{1}{2}f_+^2 - \nabla f_+\cdot\nabla\psi_+ + E\partial f_-/\partial y \quad (11)$$
$$\lim_{\rho\to\infty} g_+(\rho,y) = 0 \quad (11')$$
$$\partial g_+(a,y)/\partial\rho = -f_+(a,y)\partial\psi_+(a,y)/\partial\rho \quad (11'')$$
$$\nabla^2 f_- - f_- = \tfrac{1}{2}f_+g_- - \nabla g_-\cdot\nabla\psi_+ + E\partial g_+/\partial y \quad (12)$$
$$\lim_{\rho\to\infty} f_-(\rho,y) = 0 \quad (12')$$
$$\partial f_-(a,y)/\partial\rho = g_-(a,y)\partial\psi_+(a,y)/\partial\rho \quad (12'')$$
$$\nabla^2\psi_+ = -\tfrac{1}{2}f_+ \quad (13)$$
$$\lim_{\rho\to\infty} \psi_+(\rho,y) = 0 \quad (13')$$
$$\partial\psi_+(a,y)/\partial\rho = 0; \quad |y| > L$$
$$= -2Qe/\epsilon akT; \quad |y| \le L \quad (13'')$$

The dipole moment μ for the entire system is defined as

$$\mu = (2\pi e n_0/\kappa^4)\int_{-\infty}^{+\infty} y\,dy\int_a^{\infty}\rho f_-(\rho,y)\,d\rho \quad (14)$$

As will be shown, it is not necessary to solve eq 12 explicitly for $f_-(y,\rho)$ in order to determine the dipole moment; the integral in eq 14 can be evaluated from the differential equation. It is necessary to solve explicitly eq 9, 10, and 13. Equations 9 and 10 are conveniently solved as a pair. If eq 9 is operated on by ∇^2, eq 10 by $\partial/\partial y$, and the common $\partial/\partial y(\nabla^2 g_-)$ term eliminated, we have then for $f_+(y,\rho)$

$$\nabla^2(\nabla^2 f_+ - f_+) - E^2\partial^2 f_+/\partial y^2 = 0 \quad (15)$$

Explicitly expanding f_+ in a cosine Fourier series in y on the interval $[-C,+C]$, where C is arbitrarily large, we have

$$f_+(\rho,y) = \sum_{n=0}^{\infty} f_{+,n}(\rho)\cos(\beta_n y) \quad (16)$$

where $\beta_n = n\pi/C$. A general solution for $f_{+,n}(\rho)$, incorporating the $\rho \to \infty$ limit boundary condition, is

$$f_{+,n}(\rho) = B_1 K_0(\lambda_{1n}\rho) + B_2 K_0(\lambda_{2n}\rho) \quad (17)$$

where B_1 and B_2 are integration constants and

$$\lambda_{1n}^2 = (1 + 2\beta_n^2 + (1 - 4\beta_n^2 E^2)^{1/2})/2$$

$$\lambda_{2n}^2 = (1 + 2\beta_n^2 - (1 - 4\beta_n^2 E^2)^{1/2})/2 \quad (18)$$

the function $K_0(x)$ is a modified Bessel function of the second kind of order 0. Explicitly expanding $g_-(y,\rho)$ as a sine Fourier series ($g_-(y,\rho) = \sum_n g_{-,n}(\rho)\sin(\beta_n y)$) and using the above form for $f_{+,n}(\rho)$, the solution for $g_{-,n}(\rho)$ can be determined in terms of the constants B_1 and B_2. With the boundary conditions for $g_{-,n}(\rho)$ and $f_{+,n}(\rho)$ at $\rho = a$ ($=\kappa a'$), the coefficients B_1 and B_2 can be determined, arriving with

$$f_{+,n}(\rho) = -A_n((1 + S_n)K_0(\lambda_{1n}\rho)/(\lambda_{1n}aK_1(\lambda_{1n}a)) - (1 - S_n)K_0(\lambda_{2n}\rho)/(\lambda_{2n}aK_1(\lambda_{2n}a)))/(2S_n) \quad (19)$$

$$g_{-,n}(\rho) = \beta_n A_n E(K_0(\lambda_{1n}\rho)/(\lambda_{1n}aK_1(\lambda_{1n}a)) - K_0(\lambda_{2n}\rho)/(\lambda_{2n}aK_1(\lambda_{2n}a)))/S_n \quad (20)$$

where $S_n = (1 - 4\beta_n^2 E^2)^{1/2}$, $A_0 = 4e^2QL/\epsilon kTC$, and $A_n = 8e^2Q\sin(\beta_n L)/\epsilon\beta_n kTC$. With eq 19, eq 13 can be solved for $\psi_{+,n}(\rho)$ (expanding $\psi_+(y,\rho)$ as a $\cos(\beta_n y)$ series) to give

$$\psi_{+,n}(\rho) = A_n(K_0(\lambda_{1n}\rho)/(\lambda_{1n}aK_1(\lambda_{1n}a)) - K_0(\lambda_{2n}\rho)/(\lambda_{2n}aK_1(\lambda_{2n}a)) + S_nK_0(\beta_n\rho)/(\beta_n aK_1(\beta_n a)))/(2S_n) \quad (21)$$

Equations 11 and 12 can also be treated as a pair. Instead of explicitly solving the equations, however, the dipole moment can be evaluated by integrating eq 12 in conjunction with eq 11. In order to simply minimize the number of terms in the succeeding equations, we make the following substitutions, in addition to the Fourier expansions:

$$g_+(\rho,y) = -f_+(\rho,y)\psi_+(\rho,y)/2 + g'_+(\rho,y)$$

$$g'_+(\rho,y) = \sum_{n=0}^{\infty} g'_{+,n}(\rho)\cos(\beta_n y) \quad (22)$$

$$f_-(\rho,y) = -g_-(\rho,y)\psi_+(\rho,y)/2 + f'_-(\rho,y)$$

$$f'_-(\rho,y) = \sum_{n=1}^{\infty} f'_{-,n}(\rho)\sin(\beta_n y) \quad (23)$$

As was the case in the low-field treatment, the differential equations for f_- and g_+ are in terms of quadratic combinations of ψ_+, f_+, and g_-. As a result therefore, the nth Fourier component of either f_- or g_+ is given by mixed-mode contributions from the k and m modes of ψ_+, f_+, or g_-. We shall use the simplifying notation of $\sum_{k,m}$ to signify that the sum is over all k and m Fourier modes such that either $k + m = n$, $k - m = n$, or $m - k = n$.

With eq 22 and 23, eq 11 and 12 can be reexpressed in terms of $f'_{-,n}(\rho)$ and $g'_{+,n}(\rho)$ as

$$\nabla_\rho^2 g'_{+,n} - \beta_n^2 g'_{+,n} = \beta_n E f'_{-,n} + (1/2)\sum_{k,m}(f_{+,k}\psi_{+,m} + f_{+,k}f_{+,m}/2 - Eg_{-,k}\psi_{+,m}) \quad (24)$$

$$\lim_{\rho\to\infty} g'_{+,n}(\rho) = 0 \quad (24')$$

$$\frac{\partial g'_{+,n}(a)}{\partial\rho} = -(\psi_{+,k}(a) + f_{+,k}(a)/2)\frac{\partial\psi_{+,m}(a)}{\partial\rho} \quad (24'')$$

$$\nabla_\rho^2 f'_{-,n} - (1 + \beta_n^2)f'_{-,n} = -\beta_n E g'_{+,n} + (1/2)\sum_{k,m}(\beta_k E f_{+,m}\psi_{+,k} + g_{-,k}f_{+,m} - g_{-,k}\psi_{+,m}) \quad (25)$$

$$\lim_{\rho\to\infty} f'_{-,n}(\rho) = 0 \quad (25')$$

$$\frac{\partial f'_{-,n}(a)}{\partial\rho} = -(1/2)g_{-,k}(a)\frac{\partial\psi_{+,m}(a)}{\partial\rho} \quad (25'')$$

where $\nabla_\rho^2 = \partial^2/\partial\rho^2 + (1/\rho)\partial/\partial\rho$. If we substitute for the linear $g'_{+,n}(\rho)$ term on the right-hand side of eq 12 with the linear $g'_{+,n}(\rho)$ term on the left-hand side of eq 11 and rearrange, we can then write

$$f'_{-,n}(\rho) = -\{-\nabla_\rho^2 f'_{-,n} + E\nabla_\rho^2 g'_{+,n}/\beta_n + (1/2)\sum_{k,m}\{-(g_{-,k}(f_{+,m}/2 - \psi_{+,m}) + \beta_k E\psi_{+,k}f_{+,m} + E^2(f_{+,k}(\psi_{+,m} + f_{+,m}/2) - \beta_n g_{-,k}\psi_{+,m})/\beta_n\}\}/(1 + \beta_n^2 + E^2) \quad (26)$$

The integral that gives the dipole moment μ (eq 14) then becomes

$$\mu = (2\pi e n_0/\kappa^4)\sum_{n=1}^{\infty}\int_{-C}^{+C} y\sin(\beta_n y)\,dy\int_a^{\infty}\rho\,d\rho\,(f'_{-,n} - (1/2)\sum_{k,m}g_{-,k}\psi_{+,m}) = (2\pi e n_0/\kappa^4)\sum_{n=1}^{\infty}\int_{-C}^{+C} y\sin(\beta_n y)\,dy\int_a^{\infty}\frac{\rho\,d\rho}{(1 + \beta_n^2 + E^2)}\{\nabla_\rho^2 f'_{-,n} - \nabla_\rho^2 g'_{+,n}/\beta_n + (1/2)\sum_{k,m}\{(-2\beta_n^2 g_{-,k}\psi_{+,m} + \beta_k E\psi_{+,k}f_{+,m} - g_{-,k}f_{+,m}/2) + E^2 f_{+,k}(\psi_{+,m} + f_{+,m}/2)/\beta_n\}\} \quad (27)$$

The terms involving ∇_ρ^2 can be integrated by parts and evaluated by using the boundary conditions for $\partial f'_{-,n}(a)/\partial\rho$ and $\partial g'_{+,n}(a)/\partial\rho$ in eq 11 and 12. The rest of the integral can be evaluated in a straightforward manner by using the solutions for $\psi_{+,n}$, $f_{+,n}$, and $g_{-,n}$ in eq 19–20. The result of the integration is, as would be expected, very cumbersome, and this intermediate result will not be presented here. In order to simplify the result, the double sum $\sum_n\sum_{k,m}$ can be rewritten as just $\sum_k\sum_m$, where the summations are now over all k and m. As in ref 14, the summations can be written in the shorthand notation as

$$F(\kappa L) = \sum_{k=1}^{\infty}\sum_{m=0}^{\infty}\frac{A_k A_m}{\beta_k + \beta_m}(-1)^{k+m}F_1(\beta_k,\beta_m) + \sum_{k=1}^{\infty}\sum_{\substack{m=0\\ m\neq k}}^{\infty}\frac{A_k A_m}{\beta_k - \beta_m}(-1)^{k-m}F_2(\beta_k,\beta_m) \quad (28)$$

where the first double sum results from $k + m$ mode mixing, while the second is from $k - m$ terms. This can be reexpressed as

$$F(\kappa L) = \sum_{k=1}^{\infty}(-1)^k A_k \sum_{i=0}^{\infty}\left\{\frac{A_{2i+1}F(\beta_k,\beta_{2i+1})}{\beta_k + b_{2i+1}} - \frac{A_{2i}F(\beta_k,\beta_{2i})}{\beta_k + \beta_{2i}}\right\} + \sum_{k=1}^{\infty}A_k \sum_{i=k+1}^{\infty}\left\{\frac{A_{2i+1}F(\beta_k,\beta_{2i+1})}{\beta_k - \beta_{2i+1}} - \frac{A_{2i}F(\beta_k,\beta_{2i})}{\beta_k - \beta_{2i}}\right\} - \sum_{k=0}^{\infty}A_k \sum_{i=k+1}^{\infty}\left\{\frac{A_{2i+1}F(\beta_{2i+1},\beta_k)}{\beta_k - \beta_{2i+1}} - \frac{A_{2i}F(\beta_{2i},\beta_k)}{\beta_k - \beta_{2i}}\right\} \quad (29)$$

In the limit of $C \to \infty$, the inner sums can be approximated as the integral of a partial derivative

$$F(\kappa L) = (1/2)\sum_{k=1}^{\infty}(-1)^k A_k \int_0^{\infty} dy \frac{\partial(A_y F(\beta_k,y)/(\beta_k + y))}{\partial y} + (1/2)\sum_{k=1}^{\infty}\left\{(-1)^k \frac{A_k A_0}{\beta_k}F(\beta_k,0) + (1/4)A_k \int_{\beta_1}^{\infty} dy \frac{\partial(A_y F(y,0)/y)}{\partial y}\right\} + (1/2)\sum_{k=1}^{\infty}A_k \int_{\beta_{k+1}}^{\infty} dy \left\{\frac{\partial(A_y F(\beta_k,y)/(\beta_k - y))}{\partial y} - \frac{\partial(A_y F(y,\beta_k)/(\beta_k - y))}{\partial y}\right\} \quad (30)$$

where, in place of the A_0 coefficient of eq 20, it has been redefined in order to have the A_y series uniformly continuous at $y = 0$ as $A_0 = 8e^2QL/\epsilon CkT$. Integrating this equation, we find that the $\beta_k + \beta_m$ mode mixing terms vanish. In the limit of $C \to \infty$, the remaining $\beta_k - \beta_m$ mixed terms give for the parallel component of the ion atmosphere polarization, α,

$$\alpha_{\parallel} = \mu/E' = 2\epsilon(e^2Q/\epsilon kT)^2 F(\kappa L)/\kappa^3(1 + E^2) \quad (31)$$

where

$$F(\kappa L) = \sum_{n=1}^{\infty}\frac{1}{C}\left\{\frac{\sin(\beta_n L)}{\beta_n}\right\}^2\left\{\frac{2(1 + 8\beta_n^2 + E^2)}{(1 - 4\beta_n^2E^2 - E^4)}f_{1n} - \frac{(1 + 4\beta_n^2E^2 + E^2)^2}{2\beta_n(1 - 4\beta_n^2E^2 - E^4)}f'_{1n} - \frac{(1 + 8\beta_n^2 + E^2)}{2\beta_n(1 - 4\beta_n^2E^2 - E^4)}f'_{2n} - 2(1 + 3/E^2)f_{1n} + 2\beta_n f'_{1n} + 6(f_{2n} - 2f_{3n})/E^2\right\} \quad (32)$$

and where for arbitrary a

$$f_{1n} = \frac{1}{(1 - 4\beta_n^2E^2)^{1/2}}\left\{\frac{K_0(\lambda_{1n}a)}{\lambda_{1n}aK_1(\lambda_{1n}a)} - \frac{K_0(\lambda_{2n}a)}{\lambda_{2n}aK_1(\lambda_{2n}a)}\right\}$$

$$f'_{1n} = \frac{1 - 2\beta_n^2E^2 + E^2}{(1 - 4\beta_n^2E^2)(1 + \beta_n^2 + E^2)} + 4\beta_n E^2 f_{1n}/(1 - 4\beta_n^2E^2) + \beta_n((1 - 4\beta_n^2E^2)^{1/2} - E^2)(K_0(\lambda_{1n}a)/(\lambda_{1n}K_1(\lambda_{1n}a)))^2 - \beta_n((1 - 4\beta_n^2E^2)^{1/2} + E^2)(K_0(\lambda_{2n}a)/(\lambda_{2n}K_1(\lambda_{2n}a)))^2$$

$$f_{2n} = K_0(\lambda_{1n}a)/(\lambda_{1n}aK_1(\lambda_{1n}a)) + K_0(\lambda_{2n}a)/(\lambda_{2n}aK_1(\lambda_{2n}a))$$

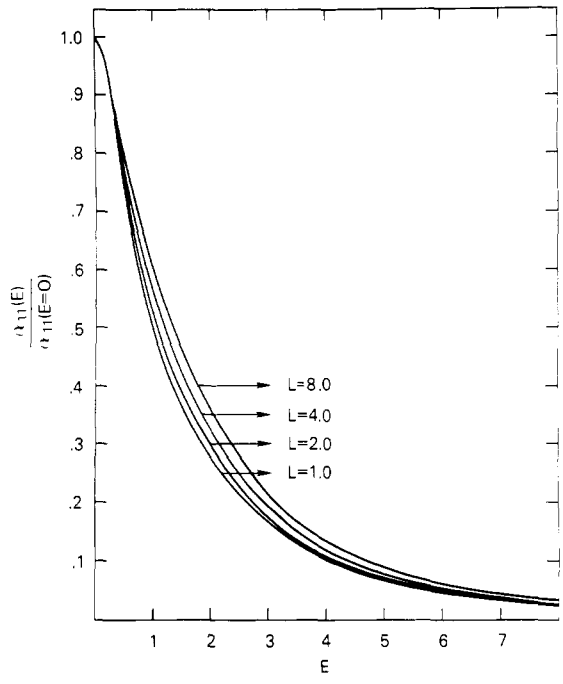

Figure 1. Parallel electric polarizability shown as a function of the reduced field strength E for four reduced rod lengths (L = 1, 2, 4, and 8) calculated from eq 31 and 32 in the thin-rod limit ($a \to 0$). In order to facilitate comparisons among different lengths, the relative polarizability $(\alpha_{\parallel}(E,L)/\alpha_{\parallel}(E = 0,L))$ is plotted.

$$f'_{2n} = -(1 + 2\beta_n^2 + E^2)/(\beta_n(1 + \beta_n^2E^2)) + \beta_n((K_0(\lambda_{1n}a)/(\lambda_{1n}K_1(\lambda_{1n}a))^2 + (K_0(\lambda_{2n}a)/(\lambda_{2n}K_1(\lambda_{2k}a))^2)/(1 - 4\beta_n^2E^2)^{1/2}$$

$$f_{3n} = K_0(\beta_n a)/(\beta_n a K_1(\beta_n a)) \quad (33)$$

For very thin rods, i.e., in the limit $a = \kappa a' \to 0$, the last set of expressions can be approximated with

$$f_{1n} = -\ln(\lambda_{1n}/\lambda_{2n})/(1 - 4\beta_n^2E^2)^{1/2}$$

$$f_{2n} - 2f_{3n} = \ln(\beta_n) - (1/2)\ln(1 + \beta_n^2 + E^2)$$

$$(K_0(\lambda a)/(\lambda K_1(\lambda a))^2 = 0 \quad (34)$$

where the $x \to 0$ limits of $K_0(x) = -\ln(x)$ and $xK_1(x) = 1$ have been substituted.

Numerical Results

The sum in eq 31 can be evaluated in a relatively straightforward manner with the aid of a computer. For dimensionless field strengths (cf. eq 8), $E > 0.05$, the sum is essentially independent of the size of the arbitrary limit C set for the Fourier expansion in the direction of the field for $C > 5000$. The terms for which $\beta_n L > 4$ contribute negligibly to the sum and mark the upper limit of n. Taking the limit of eq 31 as $E \to 0$ gives the same result as reported in our previous work. The only problem encountered in calculating polarizabilities comes in those terms in which β_n and E are large enough such that λ_{1n} and λ_{2n} are complex. From eq 18, however, if they are complex, then they are complex conjugates; i.e., $\lambda_{2n} = \bar{\lambda}_{1n}$, where the bar denotes a complex conjugate. With the relationship that $\ln(\bar{Z}) = \overline{\ln(Z)}$ (or, for the general case, $K_0(\bar{Z}) = \overline{K_0(Z)}$), each f_{in} of eq 33 and 34 is wholly real; all complex components cancel.

Figure 1 shows the progressive decrease of the calculated reduced parallel polarizability $(\alpha_{\parallel}(E)/\alpha_{\parallel}(E = 0))$ as a

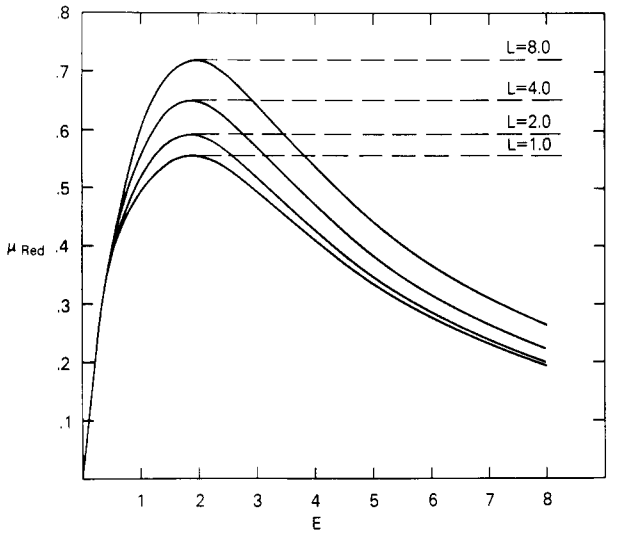

Figure 2. Reduced dipole moment μ_{red} ($=E\alpha_{\parallel}(E,L)/\alpha_{\parallel}(E = 0, L)$) shown as a function of the effective reduced field strength E for the same four lengths of Figure 1. The dashed lines illustrate the expected behavior if the dipole saturated to a field-independent value, i.e., to a permanent-like dipole moment.

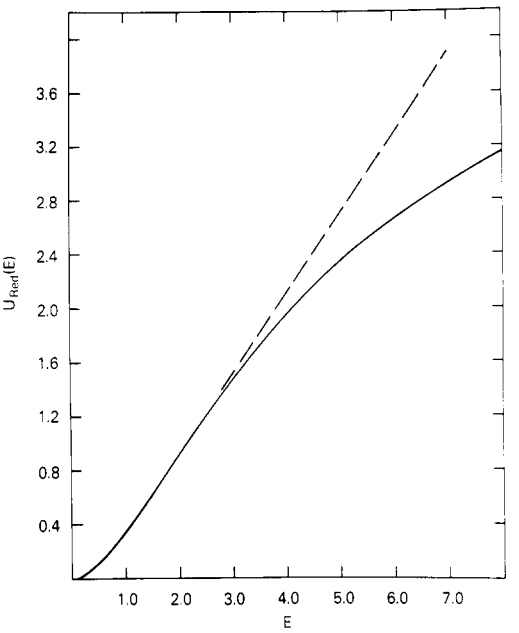

Figure 3. Dependence of the reduced dipole energy, calculated numerically from eq 36, on the effective reduced field strength E is shown for $L = 2$. The dashed line illustrates the expected curve if the dipole saturated to a field-independent value.

function of the reduced field strength for $L = 1$, 2, 4, and 8. These reduced lengths span the average range of $\kappa L'$ for salt concentrations that can be used in electric dichroism or birefringence and DNA lengths that can be considered rodlike. To a good first approximation, the functional form of the decrease is independent of the reduced length. The magnitude of the polarization is, of course, dependent on L through $\alpha_{\parallel}(E = 0)$. A more informative view of the trend in dipole properties is shown in Figure 2 for the dependence of the reduced dipole moment, $\mu_{red} = E\alpha_{\parallel}(E)/\alpha_{\parallel}(E = 0)$, on E for the four lengths in Figure 1. In contrast to most theories[7-10] that incorporate a saturation of an induced dipole for a macroion such as DNA to permanent dipole like character (i.e., the dipole moment is independent of E for large enough field strengths (qualitatively indicated by the dashed line in this figure)), the ion atmosphere polarization model indicates that μ will reach a maximal value at some field E. As the field strength is further increased past this point, the predicted dipole moment will actually begin to decrease. To within 2%, the four curves differ only by a constant factor. The actual magnitude of the dipole is related to the reduced parameter by the factor $(\kappa kT/e)\alpha_{\parallel}(E = 0)$ and, therefore, depends on the reduced length L and the ionic strength.

Just as the ion atmosphere polarization at very low field strengths has its counterpart in electrophoretic theory in the relaxation field, so also does the high-field dipole saturation have a basis in electrophoresis, the Wien effect. This effect is the experimental observation that the solution conductance or electrophoretic mobility of small ions is significantly greater at very high field strengths than at low (e.g., ref 16). The theoretical explanation of this phenomenon[17] is that at high fields the flux of ions past the central ion is very much greater than the restoring flow caused by the field of the central ion; the ion atmosphere is essentially being stripped away from the influence of the central ion, significantly reducing the retarding hydrodynamic drag of the ion atmosphere. This framework is also useful in understanding the behavior of the dipole moment with E in Figure 2. Very qualitatively, as the field strength increases, the ion atmosphere surrounding the charged, central rod is progressively stripped away from the influence of the rod. This effectively means that there will be less ion atmosphere charge left to polarize with respect to the rod, leading to a decreasing dipole moment. Our calculations show that the effect of E on the dipole moment, μ, is more prominent at lower field strengths than is the calculated Wien effect on the electrophoretic velocity. We take this as an indication that the relaxation field, which is directly related to μ, is more sensitive to E than is the hydrodynamic drag of the longitudinally symmetric ion atmosphere.

In order to calculate orientation energies, $U(E \cos \theta)$, we must explicitly include the angle θ between the applied field direction and the long axis of the rod. Assuming that the magnitude of the perpendicular dipole is much less than the parallel component, the effective field strength, E^*, can be simply defined as

$$E^* = E \cos \theta \tag{35}$$

where E is defined in eq 8 as $eE'/\kappa kT$, where E' is the actual applied field strength. With this, the expression for the reduced dipole energy takes the form

$$U_{red}(E^*) = -\int_0^{E^*} \mu_{red}(E \cos \theta)\, d(E \cos \theta) \tag{36}$$

The total energy is $U(E^*) = AU_{red}(E^*)$, where $A = (kT\kappa/e)^2\, \alpha_{\parallel}(E = 0)$. Since the four curves in Figure 2 to a good approximation differ only by a constant factor, only the $U_{red}(E^*)$ curve for $L = 2$ is shown as a function of E^* ($=E \cos(\theta)$) in Figure 3. The curve is essentially just another view of the unusual "saturation" properties of the ion atmosphere polarization model. Current treatments of the saturation of the dipole moment for a polyion such as DNA, implicitly assuming that the number of polarizable counterions is independent of field strength, indicate that the dipole moment will reach a limiting, field-independent value, i.e., permanent dipole like character. In this case, dipole energies will reach a region in which they are linearly proportional to E^*. This behavior is illustrated by the dashed line in Figure 3.

The link between these energies and experimental observations depends on the type of measurement made. For electric dichroism or birefringence, for example, the ob-

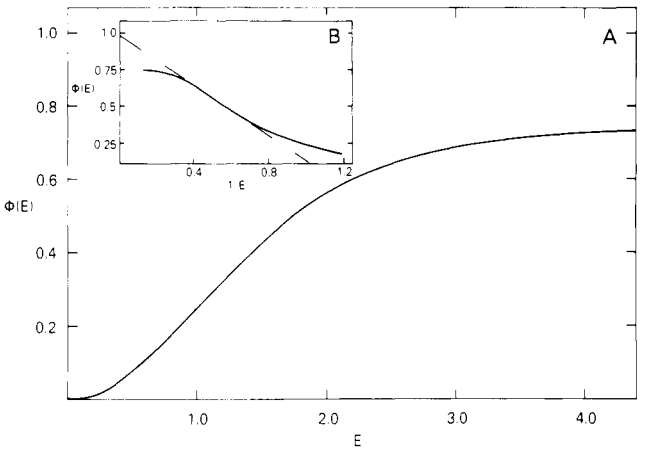

Figure 4. Dependence of the orientation function $\Phi(E)$, calculated numerically from eq 38 with $L = 2$ and $A/kT = 5$, on the reduced field strength E is shown in two commonly used ways. In (A), $\Phi(E)$ is plotted against E, while in the inset (B), $\Phi(E)$ is shown as a function of $1/E$ at high fields, a procedure that is widely used to determine the limiting birefringence or dichroism.

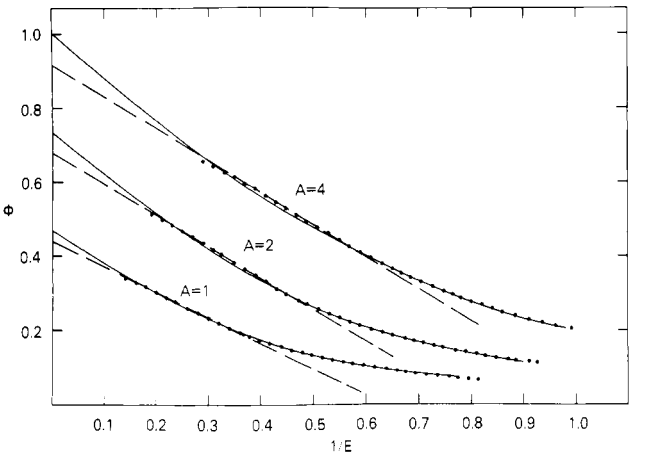

Figure 5. Effect of the saturation properties of the ion atmosphere dipole on the apparent extrapolated orientation ($\Phi(E \rightarrow \infty)$) is shown, calculated from eq 38 with $L = 2$, for three values of the coefficient A/kT (1, 2, and 4). To mimic experimental data, the theoretical calculations are presented in a pointwise manner, up to about 70–75% of the extrapolated value. The solid curves show the best quadratic in $1/E$ fits to the points, while the dashed lines are the best fits to the apparent linear terminal regions.

served change in absorbance with an applied field is proportional to the average $(\cos(\theta))^2$ projection of the rod in direction of E. The orientation function, $\Phi(E^*)$, for this system is[3,4]

$$\Phi(E^*) = \frac{\int_0^1 (1/2)(3\cos^2\theta - 1)\exp(-U(E^*)/kT)\,d(\cos\theta)}{\int_0^1 \exp(-U(E^*)/kT)\,d(\cos\theta)} \quad (37)$$

For the unusual μ vs. E behavior of Figure 3 to affect significantly the shape of the orientation curve, it is necessary that the dipole energy at the maximum μ ($E^* \sim 2$) is, at most, of the same order of magnitude as kT. Since $U_{red}(E^* \sim 2)$ is about 1, the coefficient A, relating the total energy to U_{red}, is approximately the orientation energy, in units of kT, at the maximum μ. For $A/kT = 50$, for example, a rod is virtually completely oriented at $E^* = 2$ and the effect on the orientation curve of a subsequently decreasing dipole moment will be negligible. For all practical purposes, the functional form of the Φ vs. E curve will be well described by the classical induced dipole equations. Since we are most interested in illustrating significant deviations from classical behavior, we will restrict our discussion of values of A that give orientation energies at $E^* = 2$ of the same order of magnitude as kT.

Figure 4 shows the dependence of the orientation function $\Phi(E)$ on E for $A/kT = 5.0$. For classical induced or permanent dipole moments, there are equations available that describe the entire orientation function.[3,4] For saturating dipole mechanisms, as that for DNA, there is, of course, no definitive work that can rigorously describe the observed field dependence of the dichroism. The orientation functions that are in the literature[7-10,12] assume the dipole moment saturates to a field-independent value. Empirically, a prominent feature of the observed dichroism of DNA at high field strengths is the extensive region of approximate linearity between the dichroism and $1/E$. The inset in Figure 4 shows the high-field dependence of $\Phi(E)$. As is apparent, there is here also a relatively extensive region in which the orientation function is to a good first-order approximation linearly proportional to $1/E$ (indicated by the dashed line in the inset). It is not until $\Phi(E)$ reaches about 0.75 that there is apparent a significant departure of the theoretical curve from the dashed line due to the unusual dependence of μ on E in Figure 2.

In order for the extrapolated dichroism value to be interpreted as an angle of orientation between the optical and electrical axes, it is necessary that $\Phi(E)$ extrapolates to 1.0. In the absence of a solid theoretical foundation for the form of the orientation function, an empirical, quadratic in $1/E$ fit of the experimental data at high fields is just as meaningful as any present orientation formulation. For the saturation of the ion atmosphere dipole moment, however, quadratic fits will not necessarily extrapolate to $\Phi = 1.0$. To dramatize the effect of the unusual properties of this polarization on $1/E$ extrapolations of the orientation function, Figure 5 shows pointwise calculations (to mimic experimental data) of $\Phi(E)$ for three values of A/kT (1, 2, and 4) up to field strengths that begin to show a significant departure from the apparent linear $\Phi(E)$ vs. $1/E$ region. The solid line through the points shows the best fitting quadratic approximation, while the dashed line is the best linear fit to the tail end of the data. The two simply confirm that the extrapolation in this $1/E$ range can be well approximated by a linear fit; in all three cases the difference between the two extrapolated orientations is less than about 5%. The important feature of these three curves is that they do not extrapolate to $\Phi = 1$, indicative of perfect orientation, but rather to significantly smaller values that depend on the parameter A/kT. In general, as A/kT decreases, so does the extrapolated value of the orientation function. For all three curves, the apparent linear region begins at a value of $\Phi(E)$ that is about 40–45% of the extrapolated value and continues up to about 70%. Qualitatively, this is comparable to what is observed experimentally for DNA, although some recent very high field work[12] appears to show that the dichroism remains linearly proportional to $1/E$ up to about 80–85% of the extrapolated value. As will be discussed in more detail later, our aim in this paper is simply to show that the unusual behavior of μ vs. E for the ion atmosphere polarization is qualitatively consistent with experimental observations. At this point, we are not attempting to quantitatively fit real data.

The experimental parameters that are important in defining A in aqueous solution are the Debye shielding length, $1/\kappa$ (which is proportional to $I^{1/2}$, where I is the ionic strength of the solution), and the length of the

charged rod, L'. From eq 30 and the approximation $\alpha_{\parallel}(E = 0) \sim L'^2/\kappa$,[14] for $\kappa L < 6$ (for larger *rod* $\kappa L'$ values $\alpha_{\parallel}(E = 0)$ approaches an L'/κ^2 dependence), within the framework of this limited theory, therefore, a decrease of A from 4 to 1 corresponds either to a 2-fold decrease in the rod length or to a 16-fold decrease in the salt concentration.

Discussion

When translated into physical quantities, the values of A and E that lead to the curves in Figure 5 do not correspond well to a range of DNA lengths and field strengths commonly used experimentally. From eq 30 and 31, for example, the parameters $1/\kappa = 200$ Å, $A/kT = 2$, and $E = 4$ correspond to a field strength of 47 kV/cm and a DNA length of 300 Å (~90 base pairs), assuming that $Qe^2/\epsilon kT = 1$ for a +1 ion from the Manning counterion condensation formalism. There are two major limitations in our calculations that preclude a quantitative comparison of theory and experiment. Although a Debye–Hückel treatment of the ion atmosphere surrounding a rod as highly charged as DNA is acceptable for ions about a Debye length away from the rod, it is not a good description of the ion distribution function close to the surface of the rod. The highly successful counterion condensation theory of Manning[18] assumes that the ion distribution around DNA can be split into two components: a layer of counterions bound to or condensed on DNA and then, surrounding this, the remaining charge is in a diffuse atmosphere that can be adequately treated in the Debye–Hückel approximation. The most serious shortcoming of our theory is the neglect of the polarization of the condensed layer. Ion flows of both ion atmosphere and "bound" counterions cannot correctly be treated independently. The polarization of one results in a relaxation field, in the opposite direction to the applied field, that will tend to decrease the polarization of the other. In this sense, the dipole moments of each are complementary. A decrease in one will tend to increase the other. Additionally, the polarizations of the diffuse atmosphere and the condensed layer will be interrelated by the flow of ions between the two, perpendicular to the field direction. The polarization of the condensed layer will provide a sink for diffuse atmosphere charge at one end of the rod and a source at the other. Qualitatively, however, the high-field dipole behavior of the "bound" counterions should mimic the diffuse atmosphere. The polarization will be governed by the net flux of counterions into and out of the condensed layer. The most straightforward way to overcome these problems is to drop the rather arbitrary division of ions into the condensed layer and ion atmosphere and to use a full Poisson–Boltzmann set of equations to describe the distribution and polarization of ions surrounding a highly charged, finite rod. A current view is that counterion condensation theory is just a two-state approximation to the real ion distribution that can be adequately described by the full Poisson–Boltzmann treatment.[19-21] Such a method, however, will be very difficult and lengthy, especially for high field strengths.

The second major failing of the calculations presented here is the neglect of the fact that the central rod itself will be moving due to the applied field. Including this will have two effects. First, the velocities of counter- and coions relative to the rod will be changed and, second, hydrodynamic interactions between moving charges should be introduced. The electrophoretic mobility of a macroion as highly charged as DNA is not negligible in comparison with small ions; for example, in 0.01 M Na^+, $U_{DNA} \sim 2 \times 10^{-4}$ cm^2/(s-V),[22] while $U_{Na} \sim 5 \times 10^{-4}$ cm^2/(s-V). Qualitatively, the influence of theoretically including the electrophoretic velocity will be to increase the flux of ion atmosphere charge along the rod, which is essentially equivalent to increasing the effective applied field strength. Basically, the stripping away of the ion atmosphere at high field strengths is due to ion atmosphere charge fluxes along the rod that are large compared with the forces tending to reestablish the unperturbed ion distribution. The effect of increasing this flux due to an electrophoresing rod would be to exacerbate the dipole saturation properties even further, probably shifting the calculated maximum in the dipole moment vs. E graph of Figure 2 to lower field strengths. Additionally, there are two more effects that will tend to increase the ion atmosphere flux even further. First, the electrophoretic velocity of a rod oriented parallel to the applied field, $U_{\parallel}$, should be greater than the perpendicular mobility, $U_{\perp}$.[23] As the rod orients in the field, therefore, its velocity will also increase, increasing the flux of ion atmosphere charge along the rod. Second, the stripping away of the atmosphere also means that the retarding force of the ion atmosphere on the electrophoretic velocity of the rod will decrease; i.e., the rod will move faster due to the Wien effect.

Regardless of the shortcomings of the theory, however, we believe that the results outlined in Figures 1–3 are qualitatively correct. Most importantly, they bring into question the assumption made by others[7-10,12] that the dipole moment saturates at high field strengths to a constant, field-independent value or, in other words, that the number of polarizable counterions is independent of the field strength. At least as far as a Debye–Hückel ion atmosphere polarization calculation is concerned, Figure 2 shows that the number of such "polarizable" charges is decreasing significantly at high fields, leading to the inverse dependence of the dipole moment on E observed in this figure at high enough field strengths.

There is experimental evidence that high fields do result in an extensive redistribution of the counterions surrounding DNA. Large decreases in the melting temperature (T_m) of polynucleotides that are dependent on the ionic strength have been reported.[24] Diekmann and Pörschke[25] have also observed a high-field-induced conformational change in DNA that appears to be helix melting. It is generally assumed that these decreases are due to large ionic strength dependent distortions of the helix-stabilizing ion atmosphere.[25,26] Neumann and Katshalsky[8] have reported observing conformational changes in polynucleotide structure at high field strengths that they also attribute to large helix-destabilizing distortions of the ion atmosphere. Our own experiments (unpublished observations) on +3 counterion condensed DNA[27] show that these aggregated particles can be completely disrupted with only moderately high field strengths (under 10 kV/cm). One reasonable explanation for this behavior is that enough +3 ions are being stripped away from the condensed structure that the aggregates are no longer stable.

In comparing these theoretical results with experimental data, it is of interest and importance that plots of the orientation function, Φ, vs. $1/E$ (Figure 5) do show an apparent long linear region, extending from approximately 50% of the extrapolated value all the way up to 70–80% of that value. As we have stated before, this is approximately what is observed for DNA. Hogan et al.[1] found reasonable fits to their experimental data assuming that the dipole energy goes as $E \cos^2 \theta$, which is neither an induced or permanent dipole form nor a form that can be derived from a saturated (constant at high fields) induced dipole moment. Their treatment, however, is for an ad hoc

model with the underlying physics and math left obscure. In the absence of a rigorous development of their model, it is difficult to assess whether the equation represents only an empirical fit to the data or is based on physically sound ground. Sokerov and Weill[10] have analyzed high-field data in terms of an induced dipole that saturates to a field-independent moment. Alternatively, Diekmann et al.[12] analyzed their data in terms of an induced dipole that saturates to the energy form assumed by Hogen et al. ($U \sim E \cos^2 \theta$). Both these works, however, illustrate a major failing of fitting orientation functions. Reasonable fits to the data can be achieved for a variety of dipole saturation models. As was pointed out by Sokerov and Weill, in order to extract meaningful information about dipole saturation properties, it is necessary to obtain additional information concerning the angular distribution of orientation. Electric dichroism and birefringence both measure a $\cos^2 \theta$ average of the distribution function. The insightful approach of Sokerov and Weill is to compare this average with the $\sin^4 \theta$ average that can be measured from fluorescence polarization experiments.

The major driving force behind the development of the equations in this paper was to evaluate theoretically the assumption that the polarizability saturates to a dipole moment that is independent of E, given that ions are not covalently held onto DNA. One indication that the high-field properties of polyelectrolyte polarizabilities *might* not be amendable to straightforward analysis comes from the observations of Hogan et al.[1] For short fragments of DNA, about 260 base pairs long, an apparent extrapolated dichroism, ρ_∞, of −1.2 was observed. This value is significantly less than the −1.4 to −1.5 value that would be predicted for B-form DNA as determined by X-ray diffraction.[28] Hogan et al. interpreted their low extrapolated dichroism as evidence for base pair tilting. Of greater relevance to the conclusions of this paper is the more recent work of Lee and Charney[11] and Diekmann et al.[12] Both have found that the extrapolated dichroism is dependent on the molecular weight of the DNA examined. Both groups found that for DNA fragments under about a 1000 base pairs in size, for example, ρ_∞ averages from about −1.0 to −1.25, while much larger DNA samples can give extrapolated dichroisms in the range of −1.35 to −1.45, in agreement with the X-ray work. Even the limited DNA size range examined by Hogan et al.[1] shows a small length dependence (ρ_∞ Å −1.2 for L = 230 base pairs and −1.0 to −1.1 for 140 base pairs). This dependence of ρ_∞ on the length of DNA suggests either that the extrapolation procedure for large DNA sizes is in error or that the low values are due to something other than base pair tilting. The first alternative is effectively discounted by Lee and Charney[11,19] when they find, by the same extrapolation method, that DNA in high alcohol solutions gives a ρ_∞ value that is independent of DNA molecular weight and in agreement with the X-ray structure for A-form DNA. Both Lee and Charney and Diekmann et al. interpret the observed ρ_∞ values in terms of a bent or, perhaps, "supercoiled" DNA structure. This explanation must assume two further properties of the dipole. First, for small fragments of DNA, the dipole energy gained in straightening, or, equivalently, lengthening the molecule in the field is much less than the bending energies, even at very high field strengths. Second, in order to account for the increase in ρ_∞ for very large DNAs, the dipole energy gained from straightening must increase with DNA size at a faster rate than bending energies, even though both Diekmann et al.,[12] on the basis of their empirical orientation function, and Charney and Yamaoka,[30] by fitting to a classical theoretical function, find that the apparent high field limiting, permanent-like dipole moment is only very weakly dependent on DNA length.

The results of Figure 5 suggest another possible explanation, that the low extrapolated dichroisms and molecular weight dependence do not reflect the structural organization of DNA but rather are caused by the unusual saturation properties of an induced ion atmosphere dipole.

The question of the saturation behavior of the dipole moment of highly charged polyelectrolytes like DNA is still an unsettled matter. In fact, there is as yet no entirely satisfactory theory to explain the low-field polarizability. The results of this work show that, a priori, there is no basis for assuming that the polarizability will saturate to a dipole moment that is independent of the applied field strength. For a dipole mechanism that is as incompletely understood as that for DNA, it is clear that before extrapolated dichroism values can be confidently interpreted in structural parameters, more theoretical and experimental work in characterizing the high-field electrical properties of polyelectrolytes is necessary. In addition to the already mentioned fluorescence polarization experiments, careful comparative studies on the effects of ionic strength, counterion valence, and DNA length on the high-field orientation of DNA should prove useful in determining what are the salient features of the dipole saturation.

Conclusions

The important result from our high-field calculations of the Debye–Hückel ion atmosphere polarizabilities is that the dipole moment does not saturate to a field-independent value but rather reaches a maximum value and then begins to decrease with increasing field strengths. Unlike equilibrium calculations that assume that no ions are stripped away from highly charged polyions at high field strengths, the steady-state flow approach shows that at high fields the ion atmosphere will be distorted enough to result in an apparent decrease in the number of "polarizable" ions. Trying to extrapolate experimental data at high fields for polyions that are characterized by this unusual dipole saturation behavior can result in apparent optical parameters that are not in agreement with structures determined by other methods and that are dependent on polyion length and, to a lesser extent, salt concentration.

References and Notes

(1) M. Hogan, N. Dattagupta, and D. M. Crothers, *Proc. Natl. Acad. Sci. U.S.A.*, **75**, 195 (1978).
(2) J. D. McGhee, D. C. Rau, E. Charney, and G. Felsenfeld, *Cell*, **22**, 87 (1980).
(3) C. T. Okonski, K. Yoshioka, and W. H. Orttung, *J. Phys. Chem.*, **63**, 1558 (1959).
(4) K. Yamaoka and E. Charney, *J. Am. Chem. Soc.*, **94**, 8963 (1972).
(5) D.-W. Ding, R. L. Rill, and K. E. Van Holde, *Biopolymers*, **11**, 2109 (1972).
(6) N. C. Stellwagen, *Biopolymers*, **20**, 399 (1981).
(7) M. Mandel, *Mol. Phys.*, **4**, 489 (1961).
(8) E. Neumann and A. Katchalsky, *Proc. Natl. Acad. Sci. U.S.A.*, **69**, 993 (1972).
(9) K. Kikuchi and K. Yoshioka, *Biopolymers*, **15**, 583 (1976).
(10) S. Sokerov and G. Weill, *Biophys. Chem.*, **10**, 161 (1979).
(11) E. Charney and C.-H. Lee, *J. Mol. Biol.*, **161**, 289 (1982).
(12) S. Diekmann, W. Hillen, M. Jung, R. D. Wells, and D. Pörschke, *Biophys. Chem.*, **15**, 157 (1982).
(13) J. G. Elias and D. Eden, *Macromolecules*, **14**, 410 (1981).
(14) D. C. Rau and E. Charney, *Biophys. Chem.*, **14**, 1 (1982).
(15) H. S. Harned and B. B. Owen, "The Physical Chemistry of Electrolytic Solutions", 3rd ed., Reinhold, New York, 1958, p 127.
(16) H. C. Eckstrom and C. Schmelzer, *Chem. Rev.*, **24**, 367 (1939).
(17) L. Onsager and S. K. Kim, *J. Phys. Chem.*, **61**, 198 (1957).

(18) G. S. Manning, *Q. Rev. Biophys.*, **11**, 179 (1978).
(19) M. Fixman, *J. Chem. Phys.*, **70**, 4995 (1979).
(20) M. Gueron and G. Weisbuch, *Biopolymers*, **19**, 353 (1980).
(21) R. W. Wilson, D. C. Rau, and V. A. Bloomfield, *Biophys. J.*, **30**, 317 (1980).
(22) B. M. Olivera, P. Baine, and N. Davidson, *Biopolymers*, **2**, 245 (1964).
(23) D. Stiger, *J. Phys. Chem.*, **82**, 1424 (1978).
(24) D. Pörschke, *Biopolymers*, **15**, 1917 (1976).
(25) S. Diekmann and D. Pörschke, *Biophys. Chem.*, **16**, 261 (1982).
(26) G. S. Manning, *Biophys. Chem.*, **9**, 189 (1977).
(27) R. W. Wilson and V. A. Bloomfield, *Biochemistry*, **18**, 2192 (1979).
(28) S. B. Zimmerman and B. H. Pheiffer, *Proc. Natl. Acad. Sci. U.S.A.*, **76**, 2703 (1979).
(29) C.-H. Lee and E. Charney, *Int. J. Biol. Macromol.*, **4**, *121*, (1982).
(30) E. Charney and K. Yamaoka, *Biochemistry*, **21**, 834 (1982).

Effects of Depropagation on Free Radical Copolymerization Kinetics†

Paul Meakin

E. I. du Pont de Nemours and Company, Inc., Central Research and Development Department, Experimental Station, Wilmington, Delaware 19898.
Received November 9, 1982

ABSTRACT: Three methods for calculating the effects of depropagation on free radical polymerization processes are described and compared. For the case of one depropagating monomer, all three methods (Monte Carlo simulation, "brute force" numerical integration, and a simple analytical expression for the effects of depropagation) are practical under a wide range of polymerization conditions. In this case, the analytical method is the most accurate and efficient. In the case of two (or more) depropagating monomers, we have not yet employed an analytical method, and the "brute force" method is not as broadly applicable as in the case of one depropagating monomer. However, the Monte Carlo method provides a feasible and practical way of simulating the effects of depropagation of more than one monomer on free radical polymerization, including the effects of cross-depropagation.

Introduction

Apart from a series of publications by O'Driscoll et al.[1] and an important paper by Wittmer,[2] relatively little attention has been given to the effects of depropagation reactions on free radical copolymerization processes since the early work of Lowry.[3] Most published work in this area has been concerned with the effects of depropagation on copolymer composition and sequence distribution. In this paper, three different approaches to the computer simulation of free radical copolymerization with depropagation are described and compared for the case where one monomer can undergo depropagation. These methods are (1) application of Monte Carlo methods in conjunction with numerical integration of the free radical polymerization kinetics, (2) "brute force" integration of the polymerization kinetics equations, including all free radical species of the type $R(M_1)_n\dot{M}_1$ (where M_1 is the monomer capable of depropagation) present in significant concentration, (3) numerical integration of the free radical polymerization kinetics, including a simple analytical expression for the effects of depropagation. We confine our attention to the case where the monomer(s) capable of undergoing depropagation can depropagate only if the resulting polymer radical is terminated by a monomer capable of undergoing depropagation. For example, in the case where only monomer M_1 can depropagate, the reaction $RM_2M_1\dot{M}_1 \rightarrow RM_2\dot{M}_1 + M_1$ is included, but the reaction $RM_2\dot{M}_1 \rightarrow R\dot{M}_2 + M_1$ is not permitted. For one depropagating monomer this corresponds to Lowry's case I. However, it should be noted that the approaches discussed in this paper could easily be applied in other cases.

Under the assumptions outlined above, the case of one depropagating monomer species is particularly simple since the depropagation reaction does not change the nature of the reactive free radical end group on the polymer radical. Consequently, we will first discuss the analysis of free radical polymerization kinetics with one depropagating monomer and then go on to the more general case of two or more depropagating monomers. If two or more monomers are capable of depropagation, the "brute force" integration approach is unsatisfactory under many conditions, and we have not developed a general analytical solution for the effects of depropagation. Consequently, only the Monte Carlo approach has been implemented.

One feature of our simulations is the explicit inclusion of radical–radical recombination and disproportionation reactions. This enables us to calculate monomer consumption, polymer composition, etc. under conditions where very low molecular weight polymer is being produced.

All three of our methods for simulating the effects of depropagation on free radical polymerization rely on the use of numerical methods to integrate a differential equation for the species concentrations. For this step we use a Gear algorithm.[4] In all cases, we also used standard Monte Carlo methods[5,6] to obtain monomer sequence distributions.

The basic model used in our work is one that includes initiator and monomer feed rates and initiation, propagation, depropagation, and termination reactions. The effects of other reactions such as chain transfer, thermal initiation, reaction with impurities, etc. are not considered in this paper. The specific situation simulated in the examples used in this paper is one in which initiator and monomer are fed at constant rate into a reaction vessel. The increase in volume due to addition of monomer and initiator is not taken into account. However, it would be easy to modify our computer programs to include this effect. It should also be noted that while only one po-

† Contribution No. 3121.

0024-9297/83/2216-1661$01.50/0